

# Guided interactive image segmentation using machine learning and color-based data set clustering

Adrian Friebe<sup>1</sup>, Tim Johann<sup>2</sup>, Dirk Drasdo<sup>2,3</sup>, Stefan Hoehme<sup>1\*</sup>

1 Institute of Computer Science, Leipzig University, Haertelstr. 16–18, 04107, Leipzig, Germany; 2 IfADo - Leibniz Research Centre for Working Environment and Human Factors, Ardeystrasse 67, Dortmund, Germany; 3 INRIA Paris & Sorbonne Université LJLL, 2 Rue Simone IFF, 75012, Paris, France; \*Corresponding author

**Over the last decades, image processing and analysis has become one of the key technologies in systems biology and medicine. In addition to the direct interpretation of images, the quantification of anatomical structures and dynamic processes in living systems allows for the construction of spatio-temporal models as an effective way to better understand complex mechanisms and the interplay between architecture and function. Recently, deep learning significantly improved the performance of traditional image analysis in cases where imaging techniques provide large amounts of data. In the life sciences, however, deep learning regularly proved ineffective since data sets often contain only few images and qualified annotations are not always readily available or expensive to generate.**

**We present a novel approach that combines machine learning based interactive image segmentation using supervoxels with a clustering method for the automated identification of similarly colored images in large data sets which enables a guided reuse of classifiers. Our approach solves the problem of significant color variability prevalent and often unavoidable in biological and medical images which typically leads to deteriorated segmentation and quantification accuracy thereby greatly reducing the necessary training effort. This increase in efficiency facilitates the quantification of much larger numbers of images thereby enabling interactive image analysis for recent new technological advances in high-throughput imaging. The presented methods are applicable for almost any image type and represent a useful tool for image analysis tasks in general.**

**The provided free software TiQuant makes the presented methods easily and readily usable and can be downloaded at [tiquant.hoehme.com](http://tiquant.hoehme.com).**

## Introduction

Advances in imaging technology led to a diversification of microscopy techniques enabling examination of a broad spectrum of biological questions and thus to the establishment of imaging and image analysis as one of the main pillars of bioscience. Optical microscopy in combination with (immuno)histochemical and immunofluorescent staining allows for visualization of tissue and physiological entities. Therefore, these techniques are widely used (1) in medical diagnosis, e.g. using histological sections of tissue specimens or biopsies, as a means to distinguish physiological and pathological tissue architectures, and (2) in medical research to study tissue microarchitecture, e.g. using 3D volumetric confocal microscopy [1–3], and tissue-scale or intracellular processes, e.g. by time resolved two-photon microscopy [4]. In many use-cases, computer-based image analysis is preceded by detection or pixel-accurate segmentation of objects of interest. Thereby detection asks for the location of an object in the image, e.g. using bounding boxes, while segmentation tries to capture the precise shape of the object. The most basic segmentation technique, manual pixel-accurate labeling, is time consuming, inconsistent and in many use cases, such as segmentation of e.g. blood vessels in volumetric datasets, not practically feasible. A multitude of (semi-)automatic image processing methods have been proposed, including e.g. intensity-thresholding and morphological operators [1, 3], region-based methods [5] or deformable models [6]. These methods are usually tailored towards a specific image setup (i.a. image dimensionality, magnification, staining) and/or object class (e.g. nuclei, blood vessels, necrotic tissue) and as such are typically limited in their applicability to differing use cases. Additionally, method parametrization to cope with image variability is often challenging and time consuming. More recently, shallow and deep machine learning methods were successfully applied to pixel-accurate image segmentation [7–10]. By learning object appearance from training examples these methods allow for incorporation of subtle expert knowledge, are less restricted regarding image or object class specifics and minimize parameterization complexity. Deep learning proved to be an extremely powerful approach improving performance on all tasks related to image analysis [9, 11–13]. This is mostly due to its ability of operating directly on the input image and implicitly learning features of increasing complexity. The price for finding a suitable feature space in addition to the decision surface itself is a high demand for training data and long training times. Therefore, while deep learning approaches are able to achieve superior performance their applicability in use cases with very low image counts or for interactive image segmentation is limited. In contrast, traditional, so called shallow, machine learning approaches such as random forests or support-vector machines, rely on handcrafted features. While this limits versatility, as engineered features need to represent the learning problem at hand, finding only a

decision surface in a restricted feature space greatly simplifies the learning task. Thereby, relatively few training examples and short training times are required, which makes these shallow methods eminently suitable for interactive segmentation.

A number of interactive segmentation approaches and software packages that utilize machine learning have been published in recent years. A supervoxel-based approach for segmentation of mitochondria in volumetric electron microscopy images was developed by [7], though the published executable software and code encompassed only the supervoxel algorithm *SLIC*. SuRVos [14] is a software for interactive segmentation of 3D images using a supervoxel-based hierarchy, which lays a focus on segmentation of noisy, low-contrast electron microscopy datasets. The extendable software package Microscopy Image Browser [15] allows for processing of multidimensional datasets and features a selection of conventional processing algorithms, several region selection methods aiding manual segmentation, and methods for semi-automatic segmentation, including a supervoxel-based classification approach. FastER [16] is designed specifically for cell segmentation in grayscale images, using features that are very fast to compute. The Fiji plugin Trainable Weka Segmentation [17] is a tool for pixel classification in 2D and 3D images using a broad range of features. Ilastik [18] provides a streamlined user interface with workflows for i.a. image segmentation, object classification and tracking as well as a sophisticated on-demand back end enabling processing of images with up to five dimensions that are larger than available RAM. Its segmentation workflow employs a random forest classifier for pixel classification from local features such as color, edge-ness and texture at different scales.

Most of these interactive segmentation tools allow for reuse of trained classifiers on new, unseen images. However, due to the variability of image appearance, even for sets of images that were acquired following a standard protocol, classifier reuse is usually a trial-and-error procedure and quickly becomes cumbersome for larger image sets. One of the main contributing factors to image quality variability are systematic discrepancies of colorization that can be attributed to minor deviations in the image acquisition process (e.g. sample preparation procedure, imaging settings, condition of the imaged subject). Since color information is used in various ways as a feature by all mentioned segmentation tools that target colored images, degraded prediction accuracy is to be expected for images with variational colorization.

We propose a combined approach for (i) interactively supervised image segmentation from sparse annotations and (ii) guided reuse of thereby trained classifiers on unseen images for efficient batch processing. These general methods for segmentation of two- and three-dimensional images are integrated into the image processing software TiQuant which implements various processing tools specific for liver tissue segmentation of 3D confocal micrographs as well

as the corresponding analysis functionality [1, 2]. (i) We formulate interactive pixel-accurate segmentation as a machine learning problem working on supervoxels, which are connected, homogeneously colored groups of voxels, using random forests or support vector machines as classifiers. Dimensionality reduction through use of supervoxels, precomputation of supervoxel features and a convenient graphical user interface enable rapid, intuitive refinement of training annotations by iterative correction of classification errors or uncertainties. (ii) We introduce a color-based image clustering method that enables automated partitioning of image sets into subsets of similarly colored images. A corresponding number of so-called prototype images is identified which serve as eligible candidates for interactive training of classifiers for within-subset reuse.

We evaluate the interactive image segmentation method as well as the color-based image clustering strategy to guide classifier reuse using a previously published dataset consisting of 22 brightfield micrographs of mouse liver tissue with corresponding manual nuclei annotations [3]. We show that the interactive approach outperforms a human annotator and a comparable state-of-the-art software and that limiting classifier reuse to similarly colored images greatly enhances performance compared to reuse on images of differing colorization, yielding results close to the level of a human annotator.

## Method

The general workflow of segmenting an image with our supervoxel-based approach is split from a user perspective into a preprocessing step and the interactive training, prediction and segmentation steps, that need direct user intervention and might need to be revisited iteratively for refinement in order to approach a segmentation of sufficient quality (see *Fig. 1A*).

In the preprocessing step the image is partitioned into similarly sized supervoxels and descriptive features are computed for them. A single parameter, the target supervoxel size, needs to be adjusted by the user to ensure supervoxels fit the objects of interest. This step is computationally expensive compared to the interactive steps, but is usually only performed once per dataset.

In the next step the user annotates exemplary fore- and background regions directly in the original image to generate a training database. Subsequently, a classifier is fitted to the training data and class membership probability estimates are predicted for all supervoxels of the dataset. In the final step a segmentation is generated based on the probability estimates and post-processing might be applied for refinement.

If segmentation quality is insufficient, the user can go back to the training step, to provide more training data, especially for regions that were poorly segmented. Thereby, high-quality segmentations can be quickly generated by iterative annotation refinement.

Trained classifiers can be used for prediction on unseen images, eliminating the need for producing training data for every image. However, since color descriptors are among the learned features, prediction quality on unseen images strongly depends on color similarity with the training image. By clustering a dataset of images into subsets based on their dominant colors, the process of identifying training images and qualified candidate images for classifier reuse is aided (see Fig.1B).

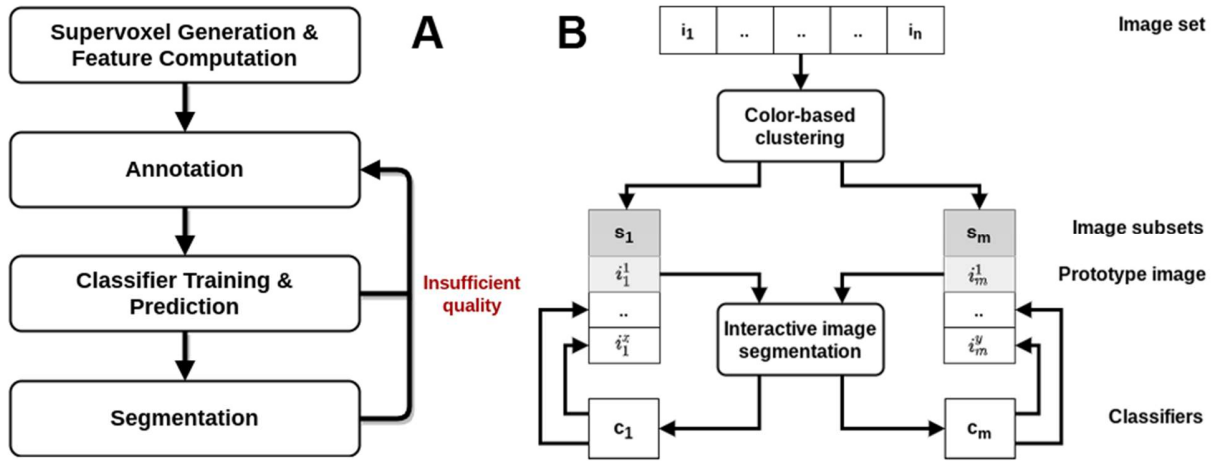


**Fig.1:** (A) Workflow of the supervoxel-based interactive image segmentation approach from a user perspective. (B) Workflow of guided reuse of interactively trained classifiers: The set of  $n$  images is clustered into  $m$  subsets of similarly colored images using our color-based image clustering method. For each subset a prototype image is identified, which is then interactively segmented. The resulting  $m$  trained classifiers are reused on the remaining images in their respective subsets.

## Supervoxel initialization

Initially, an oversegmentation into perceptually homogeneous regions, so-called supervoxels, is generated. The term supervoxel (respectively superpixel in 2D) was introduced in [8], who proposed to use oversegmentation, i.e. the process of segmenting an image so that the objects of interest themselves are split into distinct regions, as a preprocessing step to reduce image complexity while preserving most of the structure necessary for segmentation at the scale of interest. Individual supervoxels group voxels into visually meaningful building blocks, which are, depending on the chosen generative approach and parametrization, of more or less similar size and compactness. They reduce dimensionality of data without sacrificing much information, thereby greatly reducing computational cost of subsequent image processing steps and allow for

computation of local features such as color histograms and texture. To date a multitude of different supervoxel algorithms exist, which can be categorized by their high-level approach, into e.g. graph-based, density-based and clustering-based algorithms [19].

We use the *SLIC0* (“*Superpixels – IVRL*” *n.d.*) variant of the clustering-based algorithm *simple linear iterative clustering* (*SLIC*) [20], due to its comparatively strong performance regarding Boundary Recall and Undersegmentation Error [19], and its memory and runtime efficiency [20]. Its iterative nature enables straightforward runtime restriction and provides direct control over the number of generated superpixels. *SLIC* is an adaptation of k-means clustering [21] with two main distinctions: i) The search space is reduced to a region proportional to the superpixel size, yielding a complexity linear in the number of pixels and independent of superpixel number. ii) The used weighted distance measure combines color and spatial proximity, providing control over size and compactness of resulting superpixels. Its variant *SLIC0* adaptively chooses the superpixel compactness, thereby reducing free parameters to number of superpixels, or superpixel size, respectively. Examples for superpixel oversegmentations can be seen in *Fig.2*.

The algorithm was implemented as an ITK (Insight Toolkit) filter and extended to work in three dimensions. A supervoxel oversegmentation is represented by a dual data structure consisting of a list of supervoxels, which in turn are represented as lists of voxels in run-length encoding, as well as a graph in which vertices represent the supervoxels and edges signify neighboring pairs of supervoxels. Thereby, direct access to individual supervoxels, their constituent voxels, features and spatial relationships is provided.

In brightfield and confocal microscopy, tissues or physiological entities are stained; accordingly, color, color gradients or boundaries, and local color patterns are the primary source of information for image interpretation. Therefore, the implemented supervoxel features comprise local and neighborhood color histograms, edge-ness over several spatial scales, as well as texture descriptors (detailed description in *SI Appendix*), yielding a feature vector with a total of 138 entries. Feature categories can be disabled by the user to speed up processing.

## **Interactive training data generation**

For training data generation TiQuant provides a graphical user interface that allows visualization of and interaction with image data. The user can draw directly on top of the image in order to denote exemplary regions for the classes to be segmented. Supervoxels in the annotated regions are collected and their feature vector together with the annotated class are written into a training database. For examples of how training data annotation is presented within the software, see *Fig.2*.



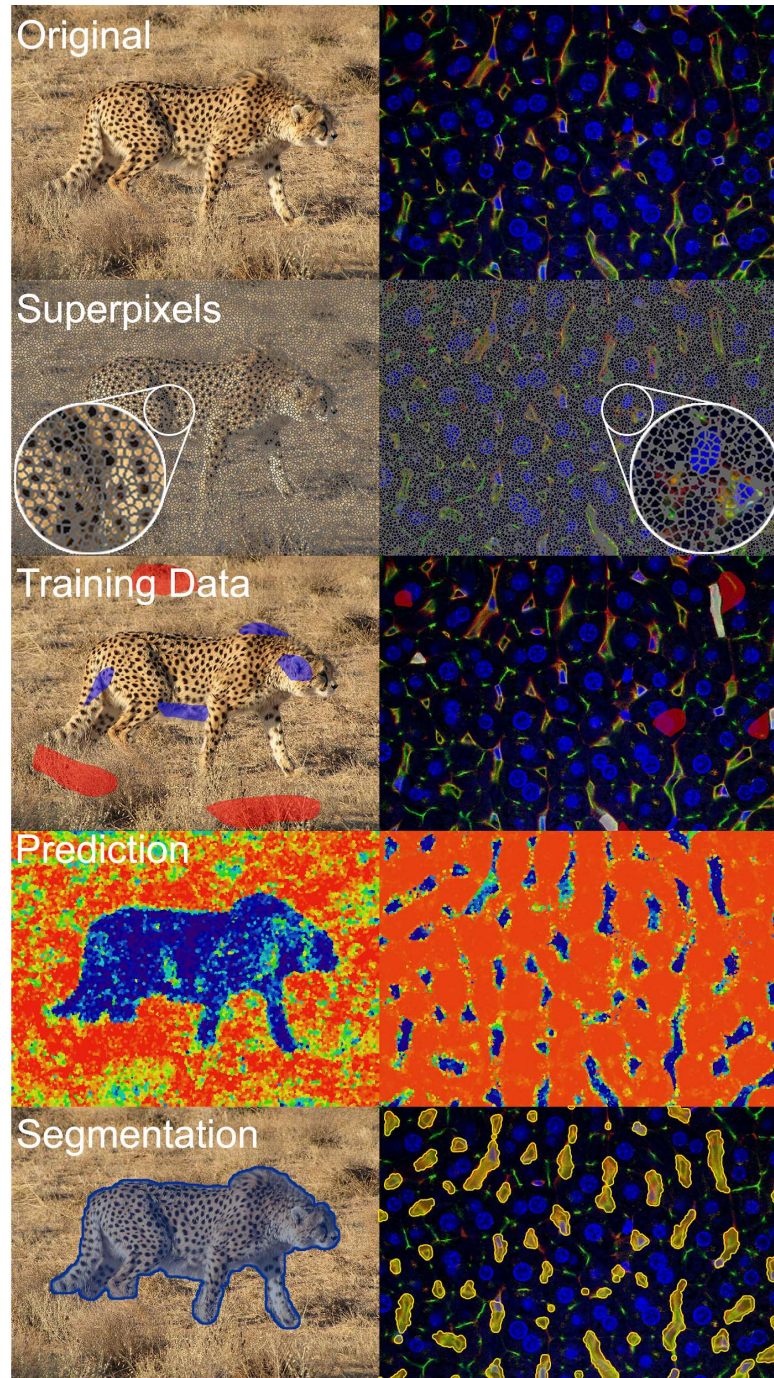


**Fig.2:** Illustration of supervoxel-based image segmentation procedure on a two-dimensional image of a cheetah in savanna in which the cheetah was segmented (left), and a three-dimensional confocal micrograph of liver tissue in which blood vessels were segmented (right). Training data for the background class is colored red in both instances, while the foreground class is colored blue in the left and white in the right example. Class membership probabilities in the prediction row are illustrated using a color mapping ranging from red (low chance of being foreground) over yellow to blue (high chance of being foreground). The segmentation is visualized by a blue overlay on the left, and a yellow overlay on the right.

## Supervoxel-Classification

Random Forests (RF) and Support Vector Machines (SVM) are supported as classifiers to learn the class membership of supervoxels given their feature vectors. We included both classifiers to choose from as they were found to be the two best-performing classifier families when evaluated on a diverse set of learning problems [22]. Furthermore, both classifier families are able to handle non-linear data and have few parameters. While RFs are faster in regard to training and execution, they can be prone to overfitting, in which case the SVM might present a better choice.

The user-supplied training data, which is summarized in the training database, is split into a training set and a test set at a ratio of 70:30 to allow evaluation of classifier performance (see *Fig.3*). Since the training data can be relatively sparse given the complexity of the learning problem at hand, we use this skewed ratio to ensure a sufficient database for training possibly at the expense of the accuracy of the classifier-performance evaluation. The split is done in a stratified fashion to ensure the preservation of relative class frequencies. Feature vectors are normalized, by subtracting mean and scaling to unit variance independently on each feature component, in order to ensure comparable feature scales.

Optionally, hyper-parameter optimization is performed on the chosen classifier to tune classifier parameters, that are not directly learnt, to the observed data patterns. In order to limit execution time while retaining the explorative quality of an exhaustive Grid Search the optimization is done using Random Search which tests a fixed number of parameter settings sampled from given distributions [23]. The search is performed on the training split with 5-fold stratified cross-validation.

In many cases user provided training data will be imbalanced, with relatively more samples of the background compared to the foreground class. To account for this mismatch, besides using the stratified version of cross-validation, training samples are weighted during the training phase, where the weight is inversely proportional to class frequency, and appropriate scoring functions are used for classifier evaluation. The Random Search algorithm used for hyper-parameter optimization uses the balanced accuracy score [24] to evaluate the performance of the optimized classifier on the test splits during cross-validation.

Additionally, SVMs are set up to provide calibrated probabilistic class membership estimates by using Platt Scaling [25], which fits an additional sigmoid function to map SVM scores to probabilities. RFs provide probabilistic estimates per default. Those can be optionally calibrated, using Platt Scaling or the non-parametric Isotonic Regression approach [26]. Empirical results show that SVMs and RFs are among the models that predict the best probabilities after calibration [27]. The Brier score was used for classifier evaluation during calibration, since it is a proper



scoring rule that measures the accuracy of probabilistic predictions and as such is a measure for calibration [28].

The (optionally) optimized classifier is trained on the training split and evaluated on the unseen test split to assess its performance. Finally, the classifier is trained and (optionally) calibrated using 5-fold cross-validation on the whole data corpus provided by the user. The resulting trained classifier is subsequently used to predict the class membership probability estimates of all supervoxels of the image. Exemplary probability maps are shown in *Fig.2*.

## Segmentation

Thresholding is applied to map the probabilistic estimates to binary class-membership, which by default is set to the value of 50%. The resulting segmentation can be post-processed using three optional filters. The first post-processing step allows for removal of isolated foreground objects smaller than a specified minimal foreground object size as well as filling of holes in foreground objects that are smaller than a minimal hole size. Additionally, a morphological closing operator followed by an opening operator can be applied to smooth surfaces. Both operators are topology preserving and thus do not separate a connected foreground object or merge disconnected foreground objects [29]. Finally, the watershed algorithm may be applied in order to split wrongly connected objects such as nuclei [30]. Two exemplary segmentations are shown in *Fig.2*.

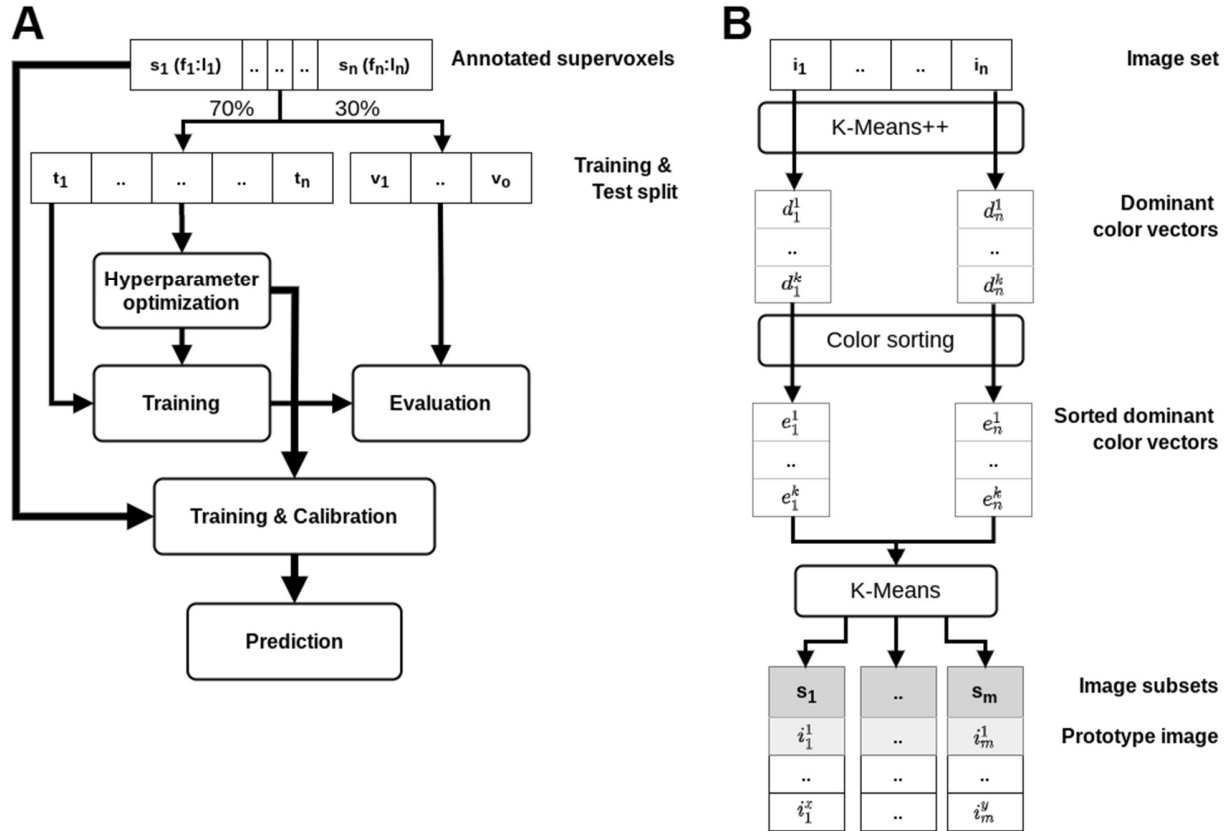


**Fig.3:** (A) Flowchart of the classifier training procedure. The set of annotated superpixels is split in a 70:30 ratio into a training and test split. Optionally, hyperparameter optimization is performed on the training split using 5-fold cross-validation. The (optimized) classifier is trained on the training split and evaluated on the test split. Finally, the (optimized) classifier is trained and calibrated on the original set of annotated superpixels 5-fold cross-validation. (B) Flowchart of the color-based image clustering algorithm. K-Means++ clustering is used to determine for each image a vector with the  $k$  most dominant colors (in RGB color space) which are subsequently sorted. Finally, K-Means clustering is applied to the sorted dominant color vectors to cluster the corresponding  $n$  images into  $m$  subsets, for each of which a prototype image is identified that is recommended for interactive segmentation.

### Color-based image clustering

A common but severe problem hampering efficient batch processing of a large number of images is visual heterogeneity of images due to varying imaging settings and conditions, or systematic visual changes during the imaged process. For example, when imaging the progression of tissue damage in liver, images with large necrotic regions are systematically visually different compared to images of healthy tissue even if all other conditions are kept constant. However, visual heterogeneity makes reuse of trained classifiers and segmentation parameterizations difficult. One approach to solve this problem are normalization methods that aim to visually equalize images before segmentation and analysis. There is a large number of normalization methods available today that typically aim at normalizing the intensity distribution of images and/or

improving the signal-to-noise ratio, such as different variations of adaptive histogram equalization [31], color deconvolution [32], or more recent deep learning based methods [33]. However, the selection of a suitable method as well as its parameterization is non-trivial. Moreover, normalization methods can easily introduce systematic errors in subsequent image analysis if differences in visual appearance originally result from changes in tissue conditions to be analyzed. In this case, normalization could remove properties that actually should be quantified.

We propose a different method to overcome the problem of visual heterogeneity in microscopic images by automatically and robustly clustering images of a given dataset into visually-homogeneous groups. Thereby, we can not only guide the selection of training images, but also facilitate classifier reuse leading to minimized manual annotation effort. The underlying assumption is that minor procedural discrepancies in the image acquisition process introduce systematic changes of coloring. Possible causes comprise slight variations between sample preparation sessions (e.g. affecting staining penetration depth, thus color saturation), minor deviations in imaging settings between imaging sessions (e.g. affecting brightness and contrast), as well as differing conditions of the imaged subjects (e.g. healthy vs. impaired tissue).

In a first step images are analyzed for their dominant colors (see *Fig.3*). This process, also known as palette design, is one of two phases of color quantization, an operation used for e.g. image compression. It has been shown that k-means clustering (Lloyd 1982) is an effective method for this task [34, 35]. In order to identify a vector of the  $k_c$  most dominant colors of an image in RGB color space, each pixel's RGB color vector is interpreted as a data point in 3D space. Instead of starting with fully random cluster centers the K-Means++ initialization scheme [36] is used, as it has been demonstrated to improve effectiveness for this task [35]. According to Lloyd's algorithm [21], each RGB-color data point is assigned to the closest cluster center and for each of the  $k_c$  resulting color clusters the cluster centers are updated as the mean of all data points assigned to them. These two steps are repeated until convergence or until a maximal number of iterations is executed, yielding a vector of the  $k_c$  most dominant colors that minimize the within-cluster variances (squared Euclidean distances).

Next, the dominant color vectors are sorted. The vectors provided by k-means clustering are ordered by color prevalence, i.e. the number of pixels that are assigned to a respective color cluster. This ordering however is susceptible to changes in image composition, so that e.g. the size or number of physiological entities influences the rank of the color cluster(s) they are assigned to. In order to make dominant color vectors of different images more comparable we sort them, which is done component-wise on the RGB vectors.

Finally, the images of a dataset are partitioned into subsets with similar dominant color vectors. Our approach extends previous work, in which color moments [37] or histograms [38] were used as image descriptors for k-means based image clustering. Each image is represented by its  $3 \cdot k_c$  dimensional sorted dominant color vector. K-means clustering is applied to this set of data points yielding  $k_i$  clusters, minimizing the within-cluster variances of the sorted dominant color vectors. The images with the smallest Euclidean distance to their respective cluster center are recommended training images for their image cluster.

## Experiments

### Validation

We validated our interactive segmentation and dataset clustering method exemplarily on a dataset consisting of 22 paraffin slices of mouse livers imaged using brightfield microscopy that were manually annotated and subsequently analyzed to study the process of tissue regeneration after intoxication with  $\text{CCl}_4$  [3]. The tissue slices were immunostained for BrdU positive nuclei to visualize proliferation and typically show a single liver lobule centered by a central vein. Image data was obtained for a control ( $t=0$ ) and at 7 different time points after administration of  $\text{CCl}_4$ , which causes a necrotic tissue damage in the area around the central vein. During the observed time period this damage is regenerated and the lost cells are replenished by cell proliferation of the surviving liver cells.

The images were originally annotated by hand by a single trained person which allows us to compare the annotation performance of a single person with the “gold standard” that is later generated by two cooperating experts. The analysis based on these manual segmentations was used in [3] for parametrization of a spatio-temporal model of the liver lobule. We reuse this dataset for method validation as it is representative for many image segmentation tasks in a biomedical context, which are characterized by small total number of available images and heterogeneous appearance of images originating in variations in sample preparation, imaging settings or tissue conditions, or various other possible technical problems like entrapped air, blurring or imperfect staining application.

A revisiting of the original annotations revealed several inaccuracies and inconsistencies (*Fig. 4A*). Therefore, two trained experts manually reassessed all 22 images thoroughly to define a final “gold standard” of manual annotation. These annotations, as the original ones, are not a pixel-wise area labeling, but rather represent each nucleus as a 2D pixel coordinate. As a measure for the accuracy of a segmentation we use the  $F_1$  score, thereby considering both precision and

recall. The underlying numbers of true positives (tp), false positives (fp) and false negatives (fn) are quantified based on an object-wise mapping of gold standard to segmentation (detailed explanation in *SI Appendix*). The measured scores are used for validation and comparison of segmentations from the original manual annotation (*Fig.4A*), our superpixel-based interactive processing approach (*Fig.4B*), intra- and inter-cluster reuse of interactively pre-trained classifiers as well as the state-of-the-art tool ilastik [18] as a reference point.

For validation of the superpixel-based approach each image was partitioned into approximately 50k superpixels of a target size of 64 pixels (initially 8x8 pixels) and each superpixel was analyzed for all available features, encompassing gradient magnitude, Laplacian of Gaussian, local and neighborhood color histograms as well as texture features.

In order to evaluate the suitability of our tool for interactive segmentation, appropriate training data was produced for each of the 22 images by annotation (following workflow *Fig. 1A*). Per image a random forest classifier was tuned using hyperparameter optimization with 5-fold stratified cross-validation, then trained and probability calibrated. The optimized and calibrated classifiers were applied to the respective image, predicting superpixel's class memberships. The corresponding segmentations were post-processed, by removing objects smaller than three superpixels, smoothing of boundaries of segmented nuclei and finally by applying the watershed algorithm to split up clusters of nuclei into individual objects.

Subsequently, to evaluate how well the trained classifiers generalize to unseen images and whether a restriction to images of similar coloring improves performance, we cluster the image set into  $k_f=6$  subsets. The number of clusters was determined experimentally using the Elbow method, which is a heuristic for determining the optimal number of clusters that represent the majority of the variability in a dataset. Image clustering uses sorted dominant color vectors with  $k_c=4$  colors, which is based on the different, size-relevant compartments (background, nuclei, and two tissue compartments for healthy tissue / necrotic lesion, or Glutamine synthetase positive / negative zone, respectively). The images with the smallest Euclidean distance to their cluster center were selected as cluster prototype images because they have the smallest average color distance from the rest of the images in the cluster and classifiers trained on them therefore are assumed to have the highest probability of good generalization performance. The previously trained classifiers of these prototype images were applied (i) *intra-cluster* to all other images in the respective cluster and (ii) *inter-cluster* to all images not belonging to the respective cluster. Segmentation post-processing was done as described before.

We compare our approach with established image processing software ilastik. For the results to be comparable, we used ilastik's 'Pixel Classification + Object Classification' workflow. All 37

predefined features were selected for training. The training annotations created with our software were imported and an object size filter was used for segmentation post-processing.

Method	median( $F_1$ )	$\sigma(F_1)$
manual	0.9021	0.027
interactive segmentation	<b>0.9297</b>	0.013
intra-cluster reuse	0.9018	0.044
inter-cluster reuse	0.6484	0.245
Ilastik [18]	0.9079	0.022

**Tab.1:** Comparison of different segmentation methods on 22 images. Bold indicates the best performance.

The summarized results of the method validation are shown in *Tab.1* while a more detailed per-image/cluster analysis is shown in the supplement *Fig.S3*. The best result was achieved by our method, when providing dedicated training data for each image. The initial manual segmentation and intra-cluster reuse of pre-trained classifiers achieved comparable scores, indicating that the

restriction of classifier reuse on similarly colored images is able to produce human-grade results, although, as the higher variance indicates, segmentation quality is less reliable. Reusing classifiers on images with differing coloring generally decreases segmentation quality greatly, as it was expected given the importance of color information. Ilastik using dedicated training data for each image performed slightly better than the pre-trained classifiers on intra-cluster images.

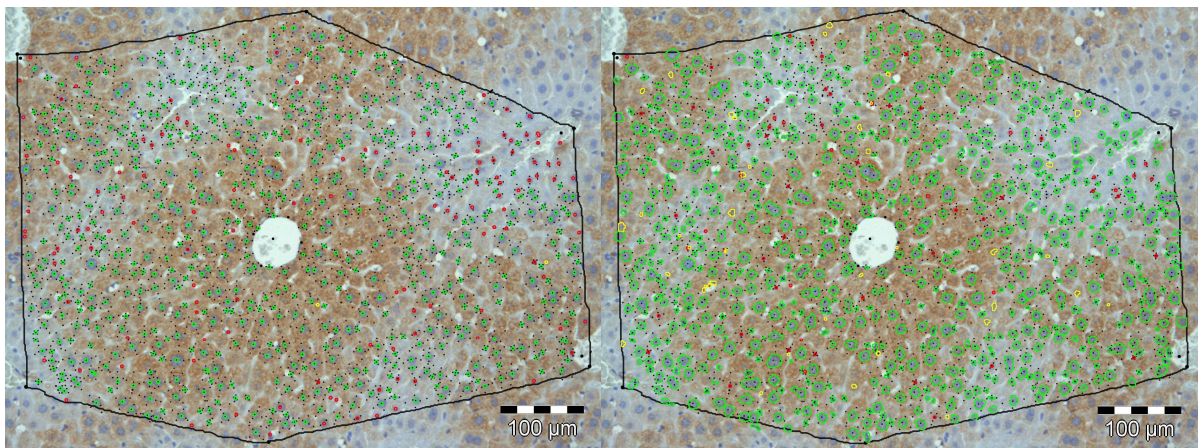


**Fig.4:** (A) Exemplary visual comparison of manual segmentation with gold standard (GS): Correctly segmented nuclei (true positives) (bright green); Incorrectly segmented nuclei (false positives) (yellow); Items not segmented as nuclei (false negatives) (red). Outlines generated from dilated 2D pixel coordinates. (B) Exemplary visual comparison of interactive segmentation with GS: Coloring as in (A). Outlines generated from object masks.

## Runtime evaluation

A detailed discussion of aspects of computational performance is given in the *SI Appendix*. The interactive processing steps training and prediction are independent of pixel count and linear in the number of supervoxels. For the segmentation step, runtime scales linear with image size and number of supervoxels. Exemplarily, execution times for an image with 100M pixels and 100k supervoxels are ~2min and 9min for supervoxel generation without and with feature generation. Training database generation, prediction and segmentation were completed in 5sec, 12sec and 51sec, respectively. The analysis was done on an Intel Core i9-7900X with 10 logical cores at a 3.3 GHz clock speed with 64 GB RAM.

## Discussion

Currently, interactive image segmentation often is the optimal image processing approach for applications where a detailed analysis of objects of interest is the aim, but only few images are available, and/or training annotations are not provided. However, these seemingly specific conditions are fulfilled in many cases of biological and medical image processing where often pixel-accurate segmentations of physiological entities are required based on two- or three-dimensional images. This includes the counting and measuring of (sub-)cellular structures and vascular networks in tissue. We find that here custom-made image processing solutions that target specific physiological entities imaged utilizing a specific technical setup are still a very common and widespread approach. Unfortunately, these solutions usually cause considerable development overhead compared to interactive solutions based on machine learning that can be easily adapted to new data through training. Moreover, custom-made solutions require profound expertise in image analysis techniques including knowledge of particular algorithms and the impact of parameter choices. In contrast, interactive image segmentation using machine learning from manual image annotations has a much flatter learning curve and greatly simplifies the process of quantifying the content of complex images enabling users to directly apply their expert knowledge of, for example, biological or medical entities in the analyzed images. The method described in this paper reduces the technical parameters virtually to zero. Solely the estimated size of the structures to be quantified is determined by the set initial size of the superpixels. In principle, even this parameter can be automatically determined (optional in the software) but usually the estimated size of the quantified structures is known.



The described advantages of interactive image segmentation hold true even if large data sets consisting of many images are available, thereby enabling deep learning. In this case, interactive image segmentation can be useful in producing training data and manual annotations with significantly reduced manual effort and thus cost.

The presented supervoxel approach using the *SLIC0* algorithm is especially suited as a basis for responsive, interactive segmentation not only because it is easy to use, but also technically due to its dimensionality reduction characteristic, minimizing processing times and memory consumption. The latter effect is particularly pronounced if the objects of interest are highly resolved. On the other hand, the advantage diminishes if object size approaches those of single pixels. For objects with fluent boundaries or low-resolution images, the alignment of supervoxels to object boundaries can be suboptimal and traditional pixel-level segmentation methods might provide higher segmentation accuracy especially in boundary areas.

The features implemented in the presented work are designed for application to color images and might be less effective in representing learning problems formulated based on grayscale or binary images, for example electron microscopy or x-ray, for which optimized features could be integrated.

Learning from annotations on single images and reusing these interactively trained classifiers for unseen images would further decrease manual effort. However, the downside of learning from such sparse annotations is a decreased generalizability which is especially deteriorating results in case of high color variations between the images to be quantified. As a solution to this problem, we demonstrated that limiting classifier reuse to similarly colored images increases average performance for the validation data set significantly, thereby improving suitability of interactive image segmentation for processing of moderately sized data sets.

## Conclusion

We present a novel approach that combines machine learning based interactive image segmentation using supervoxels with a clustering method for the automated identification of similarly colored images in large data sets which enables a guided reuse of interactively trained classifiers. Our approach solves the problem of significant color variability prevalent and often unavoidable in biological and medical images which typically leads to deteriorated segmentation and quantification accuracy when reusing trained classifiers. We demonstrate that our interactive image segmentation approach achieves results superior to both manual annotations done by a human expert and also an exemplary popular interactive segmentation tool when dedicated

training data is provided for each image (see Tab.1). We show that by limiting classifier reuse to automatically identified images of similar color properties, segmentation accuracy is significantly improved compared to a traditional, non-discriminative reuse. In addition, our approach greatly reduces the necessary training effort. This increase in efficiency facilitates the quantification of much larger numbers of images thereby enabling interactive image analysis for recent technological advances like high throughput microscopic imaging or high resolution video microscopy [39]. In summary, our approach opens up new fields of application for interactive image analysis especially in but not limited to a biological and medical context. The provided free software makes the presented methods easily and readily usable.

## References

1. Hammad S, Hoehme S, Friebel A et al. (2014) Protocols for staining of bile canalicular and sinusoidal networks of human, mouse and pig livers, three-dimensional reconstruction and quantification of tissue microarchitecture by image processing and analysis
2. Friebel A, Neitsch J, Johann T et al. (2015) TiQuant: software for tissue analysis, quantification and surface reconstruction. *Bioinformatics* 31:3234–3236.  
<https://doi.org/10.1093/bioinformatics/btv346>
3. Hoehme S, Brulport M, Bauer A et al. (2010) Prediction and validation of cell alignment along microvessels as order principle to restore tissue architecture in liver regeneration. *Proc Natl Acad Sci U S A* 107:10371–10376. <https://doi.org/10.1073/pnas.0909374107>
4. Vartak N, Guenther G, Joly F et al. (2019) Intravital multi-modal flux analysis reveals the transport mechanism of bile acids through hepatic microconduits. *bioRxiv*
5. Lopez AM, Lumbreras F, Serrat J et al. (1999) Evaluation of methods for ridge and valley detection. *IEEE Trans. Pattern Anal. Mach. Intell.* 21:327–335
6. McInerney T, Terzopoulos D (1996) Deformable models in medical image analysis: a survey. *Med. Image Anal.* 1:91–108
7. Lucchi A, Smith K, Achanta R et al. (2012) Supervoxel-based segmentation of mitochondria in em image stacks with learned shape features. *IEEE Trans. Med. Imaging* 31:474–486
8. Ren, Malik (2003) Learning a classification model for segmentation. In: *Proceedings Ninth IEEE International Conference on Computer Vision*, 10-17 vol.1

9. Ronneberger O, Fischer P, Brox T (2015) U-Net: Convolutional Networks for Biomedical Image Segmentation. In: Medical Image Computing and Computer-Assisted Intervention - MICCAI 2015. Springer International Publishing, pp 234–241
10. Ciresan D, Giusti A, Gambardella LM et al. (2012) Deep Neural Networks Segment Neuronal Membranes in Electron Microscopy Images. In: Pereira F, Burges CJC, Bottou L et al. (eds) Advances in Neural Information Processing Systems 25. Curran Associates, Inc, pp 2843–2851
11. Krizhevsky A, Sutskever I, Hinton GE (2012) ImageNet Classification with Deep Convolutional Neural Networks. In: Pereira F, Burges CJC, Bottou L et al. (eds) Advances in Neural Information Processing Systems 25. Curran Associates, Inc, pp 1097–1105
12. He K, Gkioxari G, Dollar P et al. (2017) Mask R-CNN. 2017 IEEE International Conference on Computer Vision (ICCV)
13. Long J, Shelhamer E, Darrell T (2015) Fully convolutional networks for semantic segmentation. In: Proceedings of the IEEE conference on computer vision and pattern recognition, pp 3431–3440
14. Luengo I, Darrow MC, Spink MC et al. (2017) SuRVoS: Super-Region Volume Segmentation workbench. J. Struct. Biol. 198:43–53
15. Belevich I, Joensuu M, Kumar D et al. (2016) Microscopy Image Browser: A Platform for Segmentation and Analysis of Multidimensional Datasets. PLoS Biol 14:e1002340
16. Hilsenbeck O, Schwarzfischer M, Loeffler D et al. (2017) fastER: a user-friendly tool for ultrafast and robust cell segmentation in large-scale microscopy. Bioinformatics 33:2020–2028
17. Arganda-Carreras I, Kaynig V, Rueden C et al. (2017) Trainable Weka Segmentation: a machine learning tool for microscopy pixel classification. Bioinformatics 33(15)
18. Berg S, Kutra D, Kroeger T et al. (2019) ilastik: interactive machine learning for (bio)image analysis. Nature Methods 16(12)
19. Stutz D, Hermans A, Leibe B (2018) Superpixels: An evaluation of the state-of-the-art. Comput. Vis. Image Underst. 166:1–27
20. Achanta R, Shaji A, Smith K et al. (2012) SLIC superpixels compared to state-of-the-art superpixel methods. IEEE Trans. Pattern Anal. Mach. Intell. 34:2274–2282
21. Lloyd S (1982) Least squares quantization in PCM. IEEE Trans. Inf. Theory 28:129–137
22. Fernández-Delgado M, Cernadas E, Barro S et al. (2014) Do We Need Hundreds of Classifiers to Solve Real World Classification Problems? J. Mach. Learn. Res. 15:3133–3181

23. Bergstra J, Bengio Y (2012) Random Search for Hyper-Parameter Optimization. *J. Mach. Learn. Res.* 13:281–305
24. Brodersen KH, Ong CS, Stephan KE et al. (2010) The Balanced Accuracy and Its Posterior Distribution. In: 2010 20th International Conference on Pattern Recognition, pp 3121–3124
25. Platt J, others (1999) Probabilistic outputs for support vector machines and comparisons to regularized likelihood methods. *Advances in large margin classifiers* 10:61–74
26. Barlow RE (1972) Statistical inference under order restrictions; the theory and application of isotonic regression
27. Niculescu-Mizil A, Caruana R (2005) Predicting good probabilities with supervised learning. *Proceedings of the 22nd international conference on Machine learning - ICML '05*
28. Gneiting T, Raftery AE (2007) Strictly Proper Scoring Rules, Prediction, and Estimation. *J. Am. Stat. Assoc.* 102:359–378
29. Beare R, Jackway P (2011) Parallel Algorithms via Scaled Paraboloid Structuring Functions for Spatially-Variant and Label-Set Dilations and Erosions. In: 2011 International Conference on Digital Image Computing: Techniques and Applications, pp 180–185
30. Malpica N, Solórzano CO de, Vaquero JJ et al. (1997) Applying watershed algorithms to the segmentation of clustered nuclei. *Cytometry* 28:289–297
31. Pizer SM, Amburn EP, Austin JD et al. (1987) Adaptive histogram equalization and its variations. *Computer Vision, Graphics, and Image Processing* 39:355–368.  
[https://doi.org/10.1016/S0734-189X\(87\)80186-X](https://doi.org/10.1016/S0734-189X(87)80186-X)
32. Ruifrok AC, Johnston DA (2001) Quantification of histochemical staining by color deconvolution. *Anal Quant Cytol Histol* 23:291–299
33. Litjens G, Kooi T, Bejnordi BE et al. (2017) A survey on deep learning in medical image analysis. *Med Image Anal* 42:60–88. <https://doi.org/10.1016/j.media.2017.07.005>
34. Kasuga H, Yamamoto H, Okamoto M (2000) Color quantization using the fast K-means algorithm. *Syst. Comput. Jpn.* 31:33–40
35. Celebi ME (2009) Effective initialization of k-means for color quantization. In: 2009 16th IEEE International Conference on Image Processing (ICIP), pp 1649–1652
36. Arthur D, Vassilvitskii S (2006) k-means++: The advantages of careful seeding
37. Maheshwary P, Srivastav N (2008) Retrieving Similar Image Using Color Moment Feature Detector and K-Means Clustering of Remote Sensing Images. In: 2008 International Conference on Computer and Electrical Engineering, pp 821–824
38. Malakar A, Mukherjee J (2013) Image clustering using color moments, histogram, edge and K-means clustering. *International Journal of Science and Research* 2:532–537

39. Ljosa V, Sokolnicki KL, Carpenter AE (2012) Annotated high-throughput microscopy image sets for validation. *Nature Methods* 9:637. <https://doi.org/10.1038/nmeth.2083>

Supporting Information (SI) for publication:

## Guided interactive image segmentation using machine learning and color-based data set clustering

### Supapixel features

The superpixel features comprise local and neighborhood color histograms, the averaged gradient magnitude and Laplacian of Gaussian for several sigmas, as well as texture descriptors. Histograms are calculated independently for the red, green and blue channel with each histogram having 16 bins, thus representing 4096 colors. For local histograms all pixels of a superpixel are taken into account. The neighborhood histograms additionally account for all pixels of all neighboring superpixels, thereby providing context. As a means for isotropic edge detection the gradient magnitude is computed separately for the red, green and blue channel after applying gaussian smoothing with variable sigma (0.5, 1, 2, 4, 7, 10). By varying sigma, edges of different scales are accentuated. The gradient magnitude is averaged over all pixels of a superpixel per color channel and sigma. As a second edge detection method based on the second derivative the Laplacian of Gaussian (LoG) is computed for each of the color channels and with variable sigma. The LoG is averaged over all pixels of a superpixel per color channel and sigma. Additionally, a set of six texture describing features is computed. Therefore, the RGB image is converted to a grey-level image which corresponds to the luma component Y of the YIQ color space. Based on this a grey-level co-occurrence matrix is computed which is then used to calculate the texture features [1]. Subsequently a texture feature subset comprising Inertia, Cluster Shade, Cluster Prominence, Inverse Difference Moment, Energy and Entropy as proposed by [2] is computed.

In summary, the mentioned features constitute a feature vector of 48 entries per local and neighborhood color histograms each, 18 entries per gradient magnitude and LoG values each as well as six texture descriptor entries, yielding a feature vector with a total of 138 entries to characterize each superpixel.

## Validation

Gold standard nuclei annotations are given as (center) points. True positive (tp), false positive (fp) and false negative (fn) are quantified based on an object-wise mapping of gold standard to segmentation result. A segmented nucleus is considered a tp, if a gold standard nucleus, thus its 2D coordinate, is inside the segmented area. Accordingly, a segmented nucleus for which no gold standard nucleus exists that is within its confines is considered a fp. A fn nucleus is registered, if there is no segmented nucleus in the immediate neighborhood (kernel of size 1) of a gold standard nucleus.

## Performance evaluation

We analyzed the influence of image size and superpixel number on execution times. In the first scenario the image size is successively upscaled from a 1250 x 1250 pixels image to a 15k x 15k pixel image yielding a 144-fold increase in pixel number while working with a constant number of 100k superpixels. The second scenario image size remains constant with 5000 x 5000 pixels but the number of superpixels increases stepwise from 110,835, resulting from superpixels with a target size of 15 x 15 pixels, to 4,471,427, resulting from superpixels of size 2 x 2 pixels, yielding an increase by a factor of 40.3. We evaluated for each scenario runtime of the interactive steps training, prediction and segmentation. Training used in all instances the same (scaled) training masks. Random Forest without optimization and calibration was used as classifier. The analysis was done on a Intel Core i9-7900X with 10 logical cores at a 3.3 GHz clock speed with 64 GB RAM.

Trivially, the complexity of the training step which maps the user provided training masks to superpixels and compiles the training database from those is independent from the number of pixels. The linear increase by a factor of approx. 2.6 from smallest to largest image shown in Fig.S2 can be attributed to linearly increasing image loading times. Similarly, prediction, which encompasses learning and application of the classifier to each superpixel of the image, is independent of image size as it operates directly on superpixel level. The fluctuations seen in Fig.S1 between 4.8 sec and 11.41 sec are due to differences in classifier parameterization arising during learning. Segmentation is of linear complexity regarding image size, which is confirmed showing an increase by a factor of 27.9 from 3.8 sec for the smallest to 106.1 sec for the largest image. Complexity of training, prediction and segmentation is linear in the number of superpixels due to sequential processing, which is confirmed in Fig.S2. Training times increase 28.1-fold from 3.9 sec to 109.8 sec, prediction times increase 23.5-fold from 7.9 sec to 185.6 sec and segmentation processing times increase 9.8-fold from 17.6 sec to 171.6 sec.



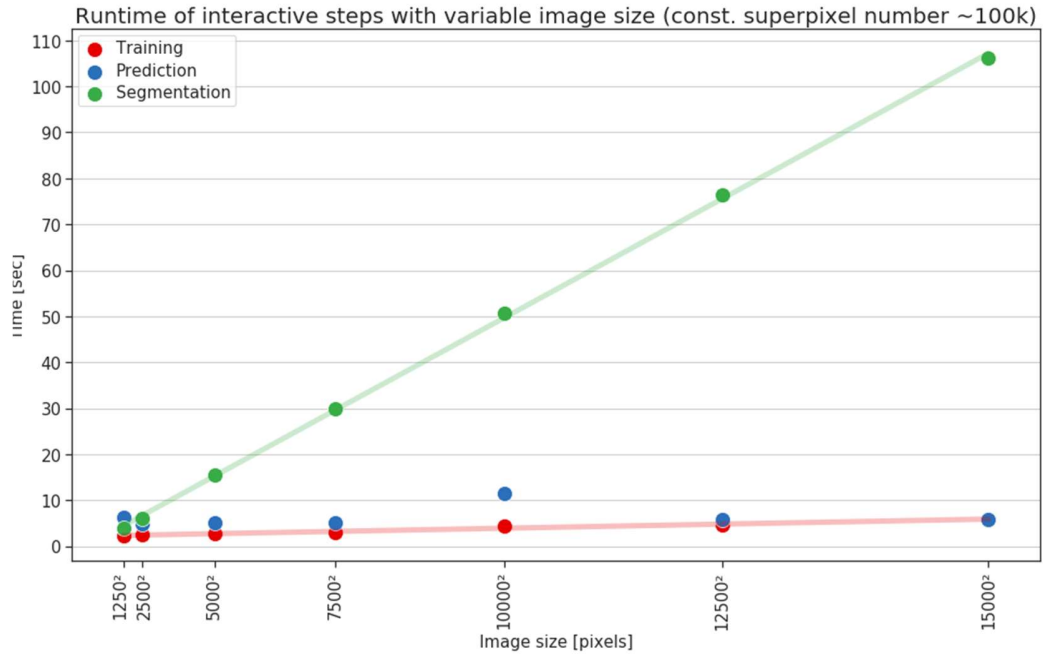


**Fig.S1:** Effect of image size on runtime of interactive processing steps. The training procedure involves identification of annotated superpixels and compilation of the training database. Prediction encompasses fitting of the classifier and prediction of class-membership probabilities for all superpixels of the image. In the segmentation step the final image is produced given the prediction results, no post-processing such as size thresholding, smoothing or watershed is applied. In all instances the same set of training annotations was used, scaled to the respective image size.

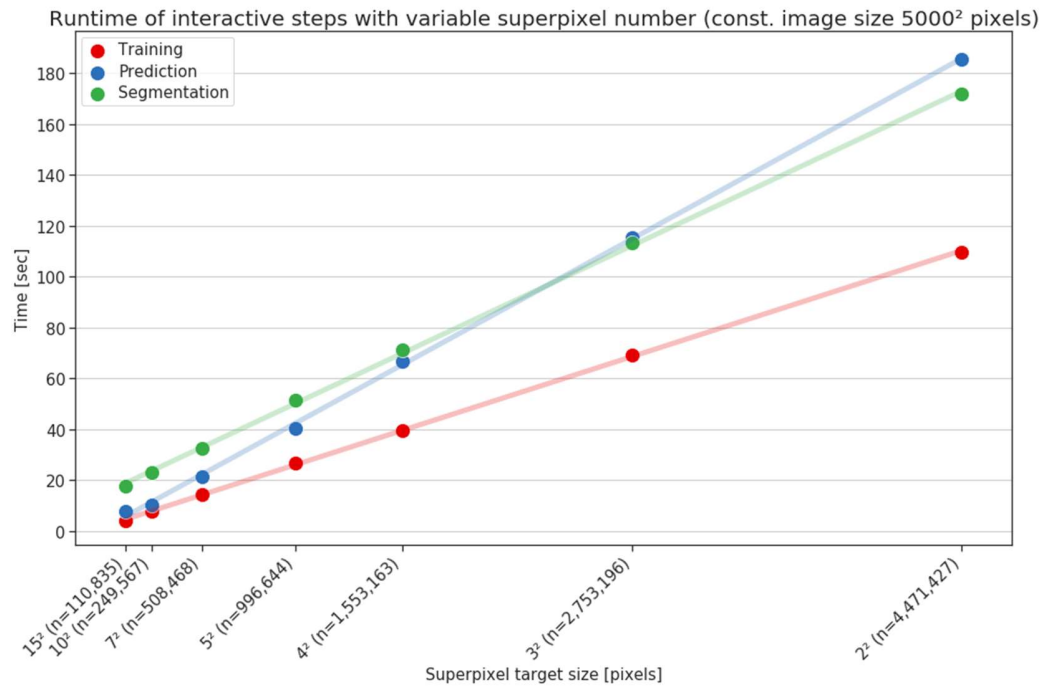


**Fig.S2:** Effect of number of superpixels on runtime of interactive processing steps. In all instances the same set of training annotations was used.

## Comparison of different segmentation methods

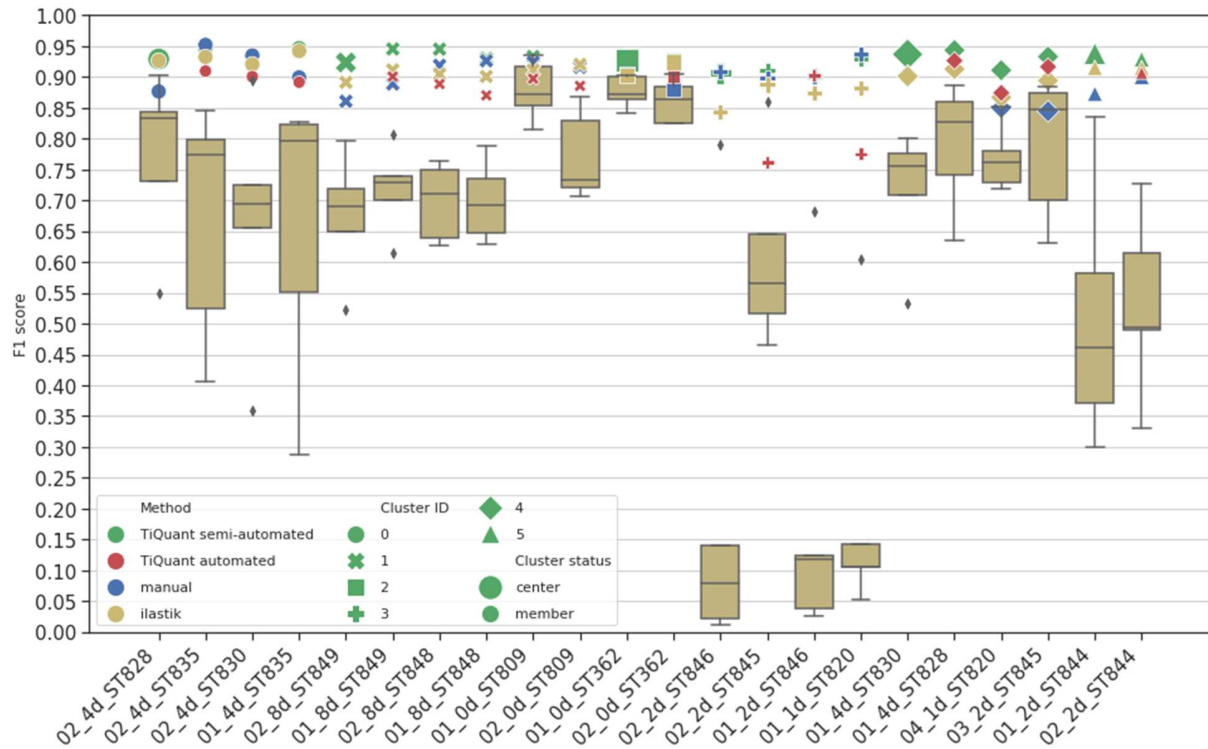


**Fig.S3:** Per image comparison of different segmentation methods: Manual annotation (blue), semi-automated superpixel-based processing (green), intra-cluster reuse of pre-trained classifier (red), inter-cluster reuse of pre-trained classifiers (box) and ilastik's 'Pixel Classification + Object Classification' workflow [3] (yellow). For intra-cluster performance analysis, the classifier trained on the cluster prototype image (leftmost) was reused on the remaining images of the respective cluster. Therefore, the cluster prototype image has no intra-cluster score. Inter-cluster performances are given as a boxplot summarizing the performance of classifiers of all other clusters.

## References

1. Haralick RM (1979) Statistical and structural approaches to texture. Proc IEEE 67:786–804. <https://doi.org/10.1109/PROC.1979.11328>
2. Connors RW, Trivedi MM, Harlow CA (1984) Segmentation of a high-resolution urban scene using texture operators. Computer Vision, Graphics, and Image Processing 25:273–310. [https://doi.org/10.1016/0734-189X\(84\)90197-X](https://doi.org/10.1016/0734-189X(84)90197-X)
3. Berg S, Kutra D, Kroeger T et al. (2019) ilastik: interactive machine learning for (bio)image analysis. Nature Methods 16(12)